24th COBEM - 2017

24th ABCM International Congress of Mechanical Engineering
December 3-8, 2017, Curitiba, PR, Brazil

COBEM-2017-2591
Design of a Low-Speed, Closed Test-Section Wind-Tunnel for Aeroacoustic and Low-Turbulence Experiments

Juan Carlos Serrano Rico
jcserrano@unipamplona.edu.co
Universidad de Pamplona, Programa Ingeniería Mecánica, Pamplona, Colombia.

Filipe Ramos do Amaral
framaral@usp.br
Christian Salaro Bresci
christian.bresci@hotmail.com
Marcello Augusto Faraco de Medeiros
marcello@sc.usp.br
Department of Aeronautical Engineering, University of Sao Paulo. Av. Trabalhador Sao-Carlense, 400. Sao Carlos, SP, Brazil. CEP 13566-590.

Abstract. *This paper shows an overview of design criteria and facility specifications of the low-speed, closed-circuit wind-tunnel located at the University of Sao Paulo, Sao Carlos School of Engineering (USP-EESC). Experimental investigations of flow-induced sound and sources of sound require an adequate environment of low-background acoustic noise and low-turbulence flow. The new wind-tunnel includes features intending to improve the flow-quality through the reduction of turbulent and acoustic disturbances and an increased flow uniformity. Such features suit the wind-tunnel for pure aerodynamic characterization as well as for aeroacoustic experiments. A long settling chamber, an hexagonal honeycomb and five nylon screens were included to minimize flow disturbances in the test-section. The turning vanes are filled with insulation, aiming the reduction and absorption of unwanted noise, whereas dense foam were installed on the corners walls, floor and ceiling to provide secondary means of background noise suppression. The wind-tunnel endue a closed test-section of* 1000×1000 *mm cross-sectional area and* 3000 *mm length, with* $7:1$ *contraction ratio. A variable-speed DC motor of* 110 *kW powers a* 13*-bladed axial fan containing* 6 *stators and the expected maximum flow-speed in the test-section is* 60 *m/s. The wind-tunnel measurement instrumentation includes a Microphone Phased Array, Particle Image Velocimetry and Hot-Wire Anemometry.*

Keywords: *Wind-tunnel, Aerodynamics, Aeroacoustics, Low-turbulence*

1. INTRODUCTION

Many wind-tunnels have been developed for the study of aeroacoustic noise, whereas advances in noise measurement techniques for anechoic wind-tunnels were achieved in the last decades Mathew *et al.* (2005); Remillieux *et al.* (2008); Chong *et al.* (2009); Devenport *et al.* (2011). Special attention has been directed to microphone phased array measurements for open and closed test-section aerodynamic wind tunnels Shin *et al.* (2007); Oerlemans *et al.* (2007). Moreover, the research community possess installations with capabilities suitable for boundary-layer stability and transition studies Hunt *et al.* (2010), and low-turbulence tunnels applied for turbulence and transition researches Lindgren (2002).

An aeroacoustic wind-tunnel design combining both a low-background acoustic noise and a low-turbulence intensity is a complex task, and only a few facilities of this kind are available around the world. Commonly, aerodynamic wind-tunnels are adapted to perform aeroacoustic experiments. This paper describes a new wind-tunnel specially designed to achieve the features addressed above, i.e., a low-background acoustic noise and a low-turbulence intensity. The *USP-EESC* closed-circuit, closed test-section, low-speed, low-turbulence, low background noise wind-tunnel was based on the results and analysis of guidelines provided in the literature Bradshaw and Pankhurst (1964); Eckert *et al.* (1976); Mehta and Bradshaw (1979); Barlow *et al.* (1999); Cattafesta *et al.* (2010).

The paper is organized as follows: Sec. 2.describes the design methodology employed, including the facility overview and details on the test-section, corners, fan, settling chamber and contraction designs; Sec. 3.shows the instrumentation available for the future experiments to be addressed in the facility and Sec. 4.summarizes the paper, including the following steps to be achieved.

2. DESIGN METHODOLOGY

2.1 Facility overview

Figure 1 shows the facility plan view. The aerodynamic circuit begins at the 3000 mm long test-section (1) with inlet measurements of 1000 mm width × 1000 mm height, whereas the outlet measures 1020 mm width × 1000 mm height. The difference between the test-section inlet and outlet cross-sections width measurements were purposeful to compensate the boundary-layer growth over the test-section walls. The test-section is followed by the diffuser 1 (2), designed to provide a pressure recovery, whereas a section of constant area between corners 1 and 2 (3) lies amid diffusers 1 and 2. A transition section, from square to circular cross-section, is connected between the diffuser 2 (4) and the fan (5) through a flexible coupling. The main drive motor has 110 kW power and is equipped with a drive speed controller to power an axial fan with 13 blades (rotor) and 16 vanes (stator). After the fan, another square to circular transition section is connected through a flexible coupling to the diffuser 3 (6). The flow leaving the third diffuser enters corners 3 and 4 (7), also showing constant cross-sectional area. A wide angle diffuser (8), housing 1 screen, follows corner 4 and the flow enters the settling chamber (9), housing 1 honeycomb and 5 removal screens to establish the flow direction and flow quality improvement. Next, the contraction (10) is achieved, with $7:1$ contraction ratio (CR), from settling chamber to test-section cross-sectional areas.

Table 1 summarizes the main features of the various wind-tunnel sections, and displays the ratio among the sections inlet and outlet cross-sectional areas. The facility overall dimensions are 18500 mm long by 8700 mm wide by 3700 mm high.

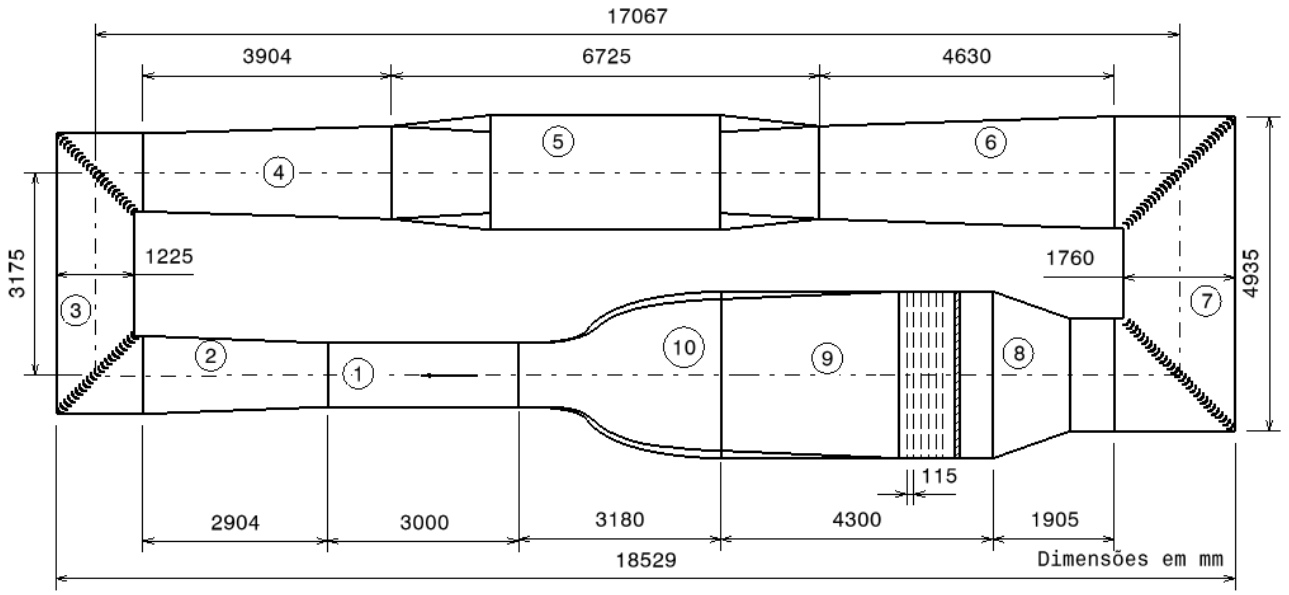

Figure 1: Wind-tunnel aerodynamic circuit. (1) test-section, (2) diffuser 1, (3) corners 1 and 2, (4) diffuser 2, (5) fan, (6) diffuser 3, (7) corners 3 and 4, (8) diffuser 4 / wide angle diffuser, (9) settling chamber and (10) contraction.

One of the main design criteria was the easy assembling/disassembling of each wind-tunnel section, as seen in Fig. 2. A modular design was chosen enabling the facility transportation to another location, as well as to allow a quick replacement of any of the sections - depending on the experimental campaign, it may be necessary to replace one or more section(s).

The wind-tunnel sections (diffusers, curves, settling chamber) were manufactured in water resistant plywood of 15 mm thickness, supported by 50 mm edge and 1.5 mm thick square cross-sections steel beams welded to

Section	**Area Ratio (Outlet / Inlet)**	**Comments**
Test-section	$1.0/1.0 = 1.0$	$L = 3000$ mm
Diffuser 1	$1.5/1.0 = 1.5$	$2\theta = 5^\circ$ $L = 2900$ mm
Corners 1 and 2	$1.5/1.5 = 1.0$	Turning vanes filled with insulation to reduce and absorb noise Surfaces with acoustic treatment (a flexible, open-cell foam from melamine resin)
Diffuser 2	$2.1/1.5 = 1.4$	$2\theta = 3.8^\circ$ $L = 3900$ mm
Fan	$2.5/2.5 = 1.0$	Fan diameter $D_F = 1800$ mm Transition sections length $L = 1700$ mm
Diffuser 3	$3.1/2.1 = 1.5$	$2\theta = 4.2^\circ$ $L = 4600$ mm
Corners 3 and 4	$3.1/3.1 = 3.1$	Turning vanes filled with insulation to reduce and absorb noise Surfaces with acoustic treatment (a flexible, open-cell foam from melamine resin)
Wide angle diffuser	$7.0/3.1 = 2.3$	$2\theta = 29.4^\circ$ $L = 1900$ mm One screen with 58% open area
Settling Chamber	$7.0/7.0 = 1.0$	$L = 4300$ mm Five screens with 58% open area One honeycomb with 3.2 mm cell diameter and 63.5 mm long
Contraction	$7.0/1.0 = 7.0$	$RC = 7$ $L = 4300$ mm

Table 1: Wind-tunnel main characteristics.

form the sections structures. To manufacture the contraction, fiberglass was employed, and the fan blades were manufactured in steel structure and fiberglass.

2.2 Test-Section

The flow out of contraction needs a distance equivalent to approximately 0.5 test-section hydraulic diameter (approximately 500 mm), for the uniformity to achieve an acceptable level Bradshaw and Pankhurst (1964). Mehta and Bradshaw (1979) suggested the test-section length may not exceed three diameters long, i.e., 3000 mm for the designed test-section, in order to avoid excessive boundary-layer growth. Nevertheless, an increase in the cross-sectional area in the downstream is sufficient to compensate for the boundary-layer growth - a strategy adopted for the designed test-section. The floor and ceiling were kept parallel while the vertical walls have a divergent angle. Figure 3 shows the test-section, which is the wind-tunnel section of lower turbulence and its configuration is fully dependent on the requirements of the experimental setup.

The test-section walls were manufactured in modules of plywood, plexiglass and foam adhered on plywood, supported by a external structure of steel beams. It has four interchangeable plexiglass windows of 10 mm thickness supported in aluminum frames, which allows an easy and quick assembling/disassembling procedure to adequate the test-section for the instrumentation needed for the experimental set. The test-section floor and ceiling are comprised of interchangeable panels, with one side made of acoustic foam and the other side made of plywood. If a quasi-anechoic environment are needed for the aeroacoustic experiments, the acoustic foam panels side may be employed. Nevertheless, for regular aerodynamic experiments, the plywood panels side are

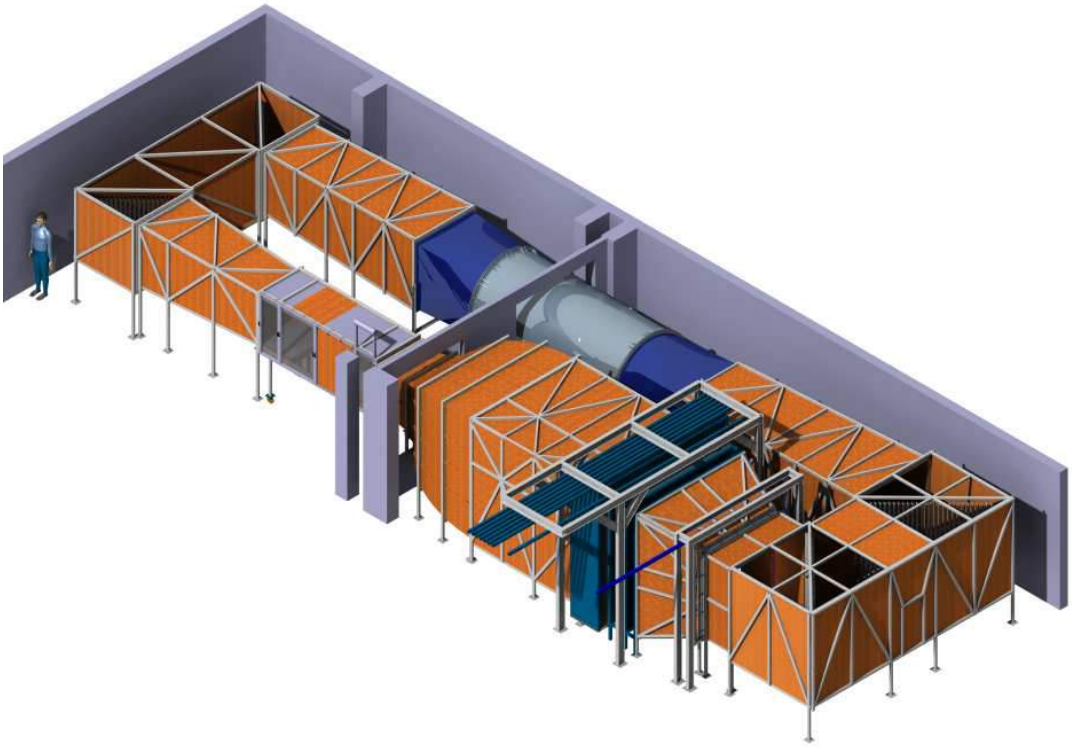

(a) Assembled wind-tunnel overview

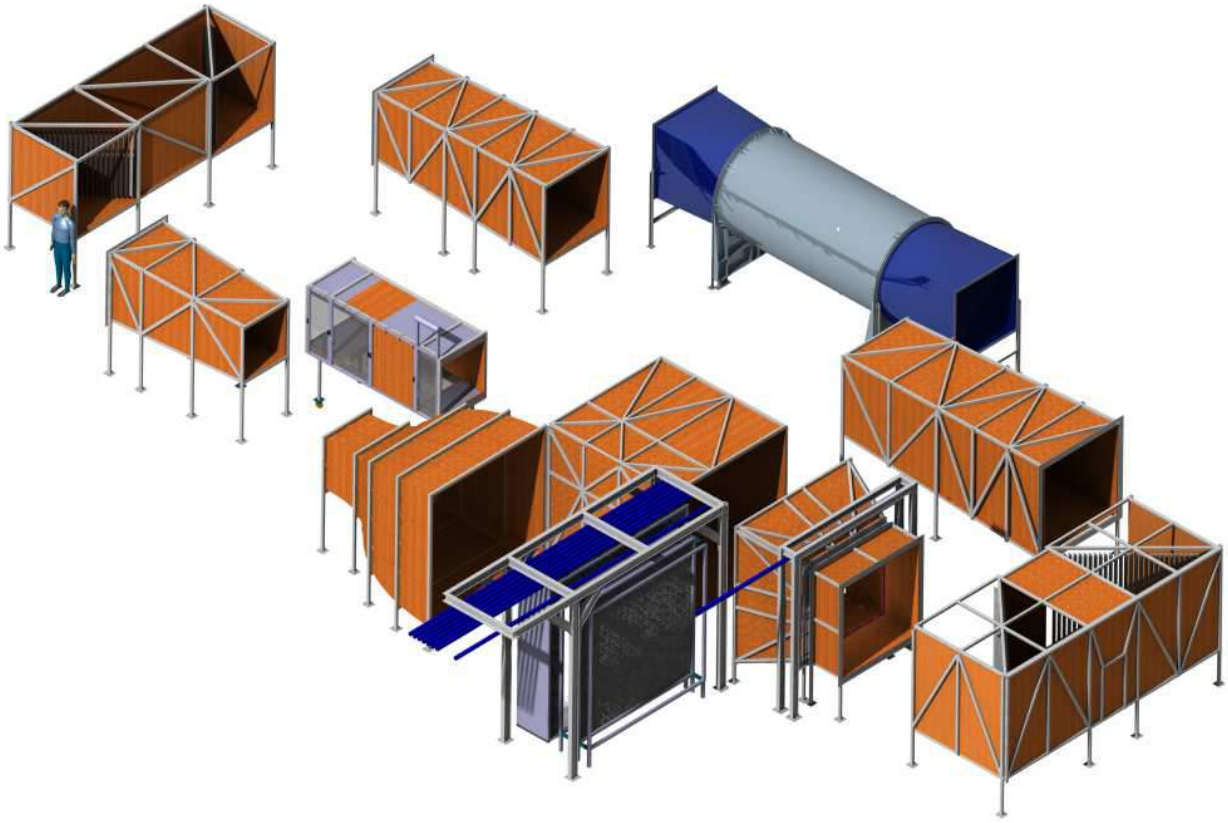

(b) Modular structures

Figure 2: Wind-tunnel design.

(a) Test-section design (b) Picture of the assembled test-section

Figure 3: Wind-tunnel test-section.

assembled. Two floor/ceiling panels of plexiglass are available for *PIV* experiments, providing access for the video camera and/or laser. A breather was included at the test-section outlet to force the pressure at this point near the room pressure, i.e., approximately 1 atm. Wheels and quick-fit mechanisms facilitate the uncoupling of the test-section from the wind-tunnel, to enable the test model installation and test-section exchange.

2.3 Corners

The corners are employed to deflect the air flow by 90° with minimal pressure losses and flow disturbance. Their internal plywood walls are covered with *BASF* acoustic melamine -based foam of 100 mm thick, Fig. 4. Over the foam surface, a black polyurethane film was applied to prevent foam erosion owing the flow that passes through it. The *Ductmate* turning vanes are manufactured in steel and filled with an insulation material aiming noise absorption. In order to securely hold and position the turning vanes, top and bottom rails were installed. They insure a precise vane alignment, quick assembly and easy means of securing turning vanes. Fig. 4(a) shows the corner 1 with no acoustic foam and turning vanes installed, whereas Fig. reffig: curves(a) shows the same corner after the installation of such noise reduction devices.

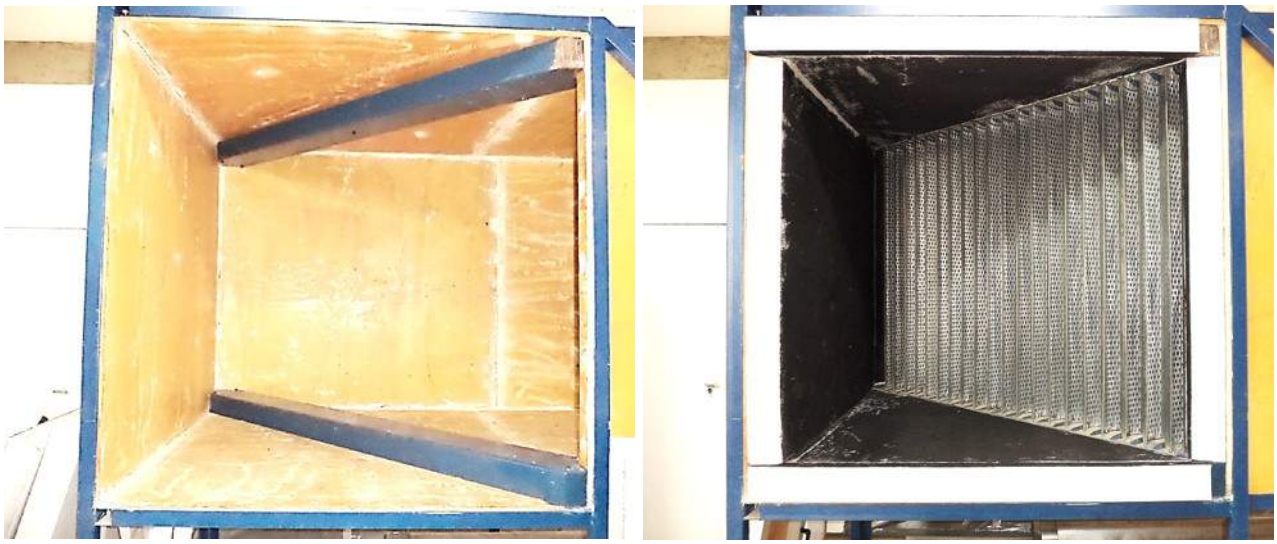

(a) After (b) Before

Figure 4: Pictures of corner 1 after and before the installation of the turning vanes and acoustic foam.

2.4 Diffusers

The diffusers are employed to decrease the flow speed, to recover the static pressure drop and to keep the drive system load as efficiently as possible Bradshaw and Pankhurst (1964). To prevent flow separation over the walls, which may induce pressure fluctuations and turbulence in the test-section, the diffuser cross-sectional area should increase gradually along its axis. The divergent angle should not exceed 5° for a better flow steadiness and flow separation control, whereas 10° is the highest recommended divergent angle to achieve the largest pressure recovery. As for the inlet-outlet cross-sectional area ratio, it should not exceed 2.5 Mehta (1977). Such criteria were adopted for the design of diffusers 1, 2 and 3. Access doors were implemented in the vertical walls of those three diffusers in order to facilitate maintenance procedures. Figure 5(a) displays a picture of diffuser 1, installed between the test-section and corner 1.

The wide angle diffuser is employed to minimize the length of the wind-tunnel if a large area ratio contraction is necessary. Such a wide angle diffuser is installed before the settling chamber. Its cross-sectional area inlet-to-outlet is so high that flow separation can be avoided only through boundary-layer control Mehta (1977), and the most common method to avoid the flow separation is to install one screen at the diffuser inlet. The designed wide angle diffuser, Fig. 5(b), contains one screen, the same as those employed in the settling chamber. The screen characteristics will be discussed in Sec. 2.5

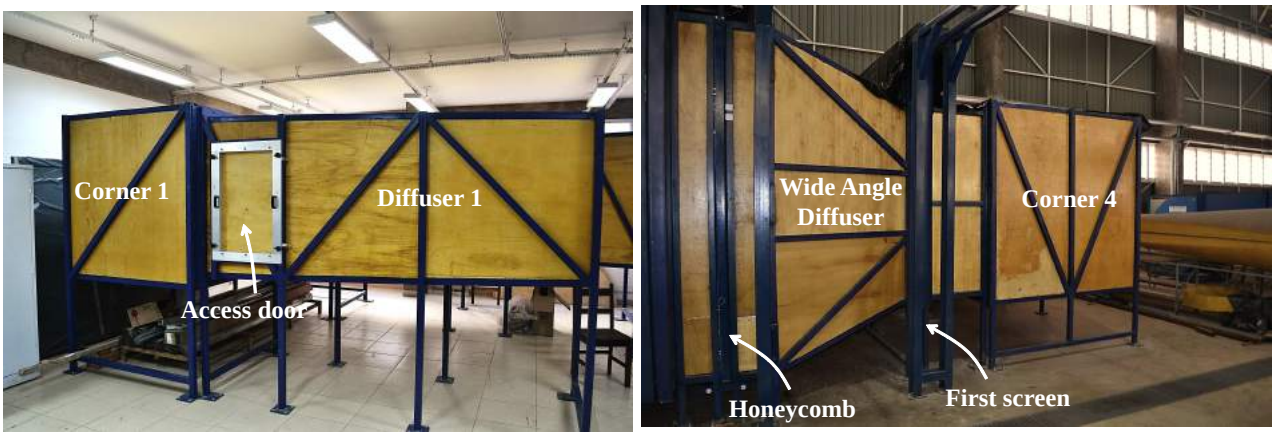

(a) Diffuser 1

(b) Wide angle diffuser

Figure 5: Pictures of wind-tunnel diffusers.

2.5 Settling Chamber

The flow field is affected along the wind-tunnel circuit, e.g., by the fan and corner vanes geometries. The settling chamber aims at providing a low-turbulence flow, parallel to the tunnel center axis and spatially uniform. Such a section, Fig. 6(a) has the larger wind-tunnel cross-sectional area and the lower flow speed. It is a suitable section to install devices to improve the flow quality, owing the minimum pressure drop, which reduces the fan power consumption. The flow conditioning elements usually consists of a honeycomb, Fig. 6(b), and screens, Fig. 7. The number of screens are dependent on the turbulence level requirements in the test section. The honeycomb is the most efficient device to straighten the flow and to suppress the lateral components of turbulence, whereas the screens are employed to reduce spatial fluctuations in the axial velocity and turbulence. Honeycomb and screens are usually combined, as the screens are not as effective as the honeycomb to straighten the flow Scheiman and Brooks (1981).

A rail and drawer mechanism is employed to dock the screens and honeycomb on the settling chamber and to facilitate maintenance/removal procedures, including individual adjustment of the screens tensioners and cleaning. The first screen, measuring 1700 mm width and 1700 mm height, is docked between corner 4 and the wide angle diffuser and is employed to prevent flow separation owing the drastic cross-sectional area increase (and consequent high pressure drop) between these sections, as discussed in Sec. 2.4 The 4300 mm long settling chamber is equipped with one honeycomb and five parallel high-tension screens, yet it is possible to increase the number of screens up to seven, each one measuring 2600 mm width and 2600 mm height.

The screens dimensions are determined by the *Reynolds* number (Re_d) based on the wire diameter (d), the mesh size (M_s) and the porosity (β_s). The nylon screen selected shows a porosity $\beta_s = 0.58$ (for $M_s = 22$), and a

(a) Settling chamber outside view - from left to right: contraction, settling chamber main section, screens dock, honeycomb dock and wide angle diffuser

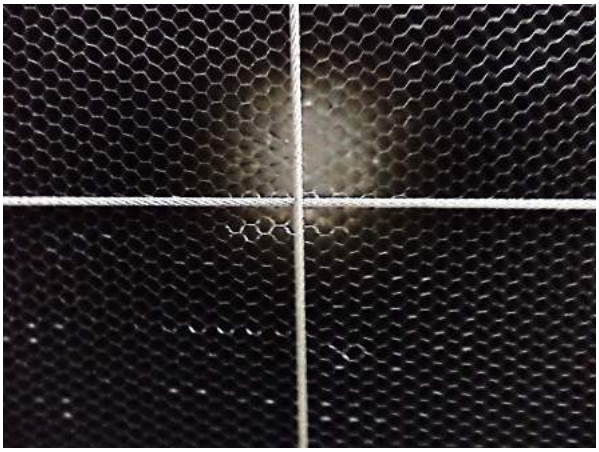

(b) Hexagonal honeycomb - detail on the stainless steel wire rope employed to secure the honeycomb panels from disassembling

Figure 6: Pictures of the settling chamber and its flow conditioning devices.

(a) Half docked wide-angle diffuser screen

(b) Undocked settling chamber screens

Figure 7: Pictures of the screens employed to conditioning the flow.

wire diameter $d_s = 0.31$ mm (for $Re_d > 100$, super-critical condition). For this set of parameters, the small scale turbulent structures are generated by the screen wires. The flow disturbances reduction are lower for super-critical than sub-critical screens and it is preferable not to employ sub-critical screens owing its larger pressure drop, which leave them susceptible to dirt contamination as well as the sub-critical screens mesh are more expensive Groth and Johansson (1988). A distance larger than 30 mesh sizes among the parallel screens are employed to achieve a sufficient decay of the wire generated turbulence Groth and Johansson (1988). The spacing between the first and second screens, and second and third screens is 230 mm, whereas the spacing between the other screens is 120 mm.

The honeycomb, measuring 2600 mm width and 2600 mm height, is manufactured in panels of aluminum hexagonal -shaped cells, with 3.2 mm cell diameter and 63.5 mm cell thickness (length). The cell length to diameter ratio (L_{HC}/D_{HC}) is approximately 20. A honeycomb with 10 cell diameters length is recommended Bradshaw and Pankhurst (1964) as an effective flow straightening device. A stainless steel wire rope of 1.587 mm diameter was tied closely to the honeycomb downstream side to secure the panels from disassembling with the flow speed.

2.6 Contraction

The contraction aims at increase the flow mean velocity and produce a uniform flow of low-turbulence intensity. Many authors have been interested in methods of designing low-speed wind-tunnel contractions Morel (1975); Watmuff (1986); Bell and Mehta (1988). Once the contraction ratio is chosen, the most important design

parameters are its length and the wall shape. The design procedure intent to avoid flow separation over the contraction walls and to produce a uniform flow with the shortest contraction possible. Whitehead *et al.* (1951) propose an analytical method to design contractions, which solves the flow in the *hodograph plane*, employing the velocity potential and stream function as independent variables to define the contraction wall shape.

(a) Contraction design (b) Contraction picture taken from the inside of the settling chamber

Figure 8: Contraction employed to induce a flow acceleration from the settling chamber to the test-section.

The designed contraction, Fig. 8, is short to minimize the boundary-layer growth and to prevent the laminar boundary-layer separation associated with the adverse pressure gradient on the contraction wall of higher curvature. Corner fillets of 45°, Fig. 8(b), were employed to reduce secondary flows induced through the interaction among the boundary-layers of the contraction vertical walls, ceiling and floor. The fillets dimensions decrease from a initial value of 150 mm × 150 mm at the contraction inlet to 0 mm over its outlet.

2.7 Fan

The fan, Fig. 9, provides a volumetric flow-rate up to 60 m^3/s and a correspondent static-pressure loss compensation, and is a significant source of acoustic background noise. The noise generated by an axial fan usually consists of two components: the turbulent noise (of broadband -like characteristic) and the discrete frequency noise (of tonal -like characteristic). Both components are generated either by the rotor (rotor self noise) or by the interaction between rotor and stator (rotor-stator interaction noise) Fukano *et al.* (1977).

Its main design parameters aims at minimize the noise generation, as the fan shows a lower *rpm*, tip clearance gap, and relationship between rotor and stator number of blades Tyler and Sofrin (1962). The rotor consists of 16 blades manufactured in fiberglass and reinforced with steel sheets, whereas the stator comprises 13 fiberglass vanes. The axial fan of 1800 mm external diameter and 680 mm hub diameter is driven by a 110 kW *Siemens* electric motor and controlled by a *Siemens Micromaster 440* variable frequency drive.

To minimize structural vibrations and acoustic contaminations, the fan was isolated from diffusers 2 and 3 through a 100 mm flexible coupling. The fan housing was assembled on a large and isolated concrete slab, with a plate attached to the bottom of the structure and secured by anchor rods. Rubber pads are also included between the plates and the floor.

3. INSTRUMENTATION

The low-speed wind-tunnel was designed for aeroacoustic and aerodynamic experiments. The test-section static and dynamic pressures are measured with a *Dwyer* Pitot tube, connected to a *Dwyer series 475 Mark III* hand held digital manometer. A *k-type* thermocouple is employed to assess the flow temperature and a portable *Instrutemp ITWH1170* weather station provides the atmospheric temperature and pressure. The assessment of the parameters above enable the flow speed calculation in the test-section.

The aeroacoustic experiments are intended to locate the acoustic sources on a test model and to quantify the noise

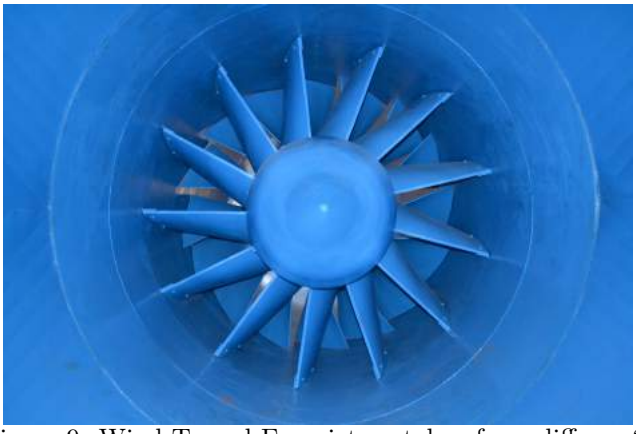

Figure 9: Wind-Tunnel Fan picture taken from diffuser 2.

spectrum associated with those sources of sound. Our research group has a long experience with aeroacoustic experiments Amaral *et al.* (2014); Pagani (2014); Amaral *et al.* (2015, 2016); Pagani *et al.* (2016); Amaral *et al.* (2017); Pagani *et al.* (2017). For the acoustic measurements, a phased array of 112 *G.R.A.S. Sound and Vibration 1/4" 40PH* microphones was designed, Fig. 10, to be mounted on the test-section windows. The microphones reach frequencies up to 20 kHz and have a large dynamic range topping at around 135 dB. The data acquisition is achieved with a *National Instruments* hardware, including five *PXI-4496* and two *PXI-4498* boards of 24-bit 16 analogical inputs arranged into a *PXI-1042Q* chassis. Data transfer is accomplished at 132 MB/s by the *PXI-PCI8336 modulus*, which connects the *PXI-1042Q* chassis and the *PXI-8351* computer.

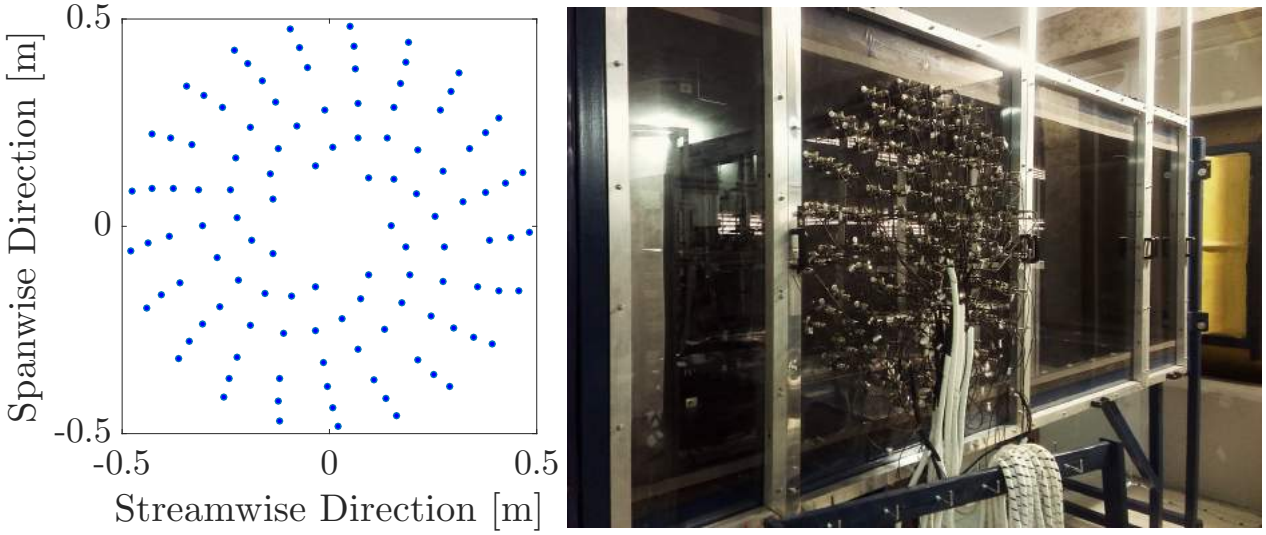

(a) Microphone phased array design

(b) Antenna mounted on the test-section window

Figure 10: Microphone array employed for the aeroacoustic experiments.

Particle Image Velocimetry, *PIV*, is a non-intrusive technique for indirect inference of the flow field over gaseous or liquid flows. Unlike the hot-wire anemometry technique, which infers the flow speed at only one point in space through the heat transfer rate from the fluid to a heated probe, the *PIV* shows results for a full scanning field. The velocity vectors are measured over the displacement of the particles that follow the movement of the fluid and their rate of movement is perceived through the recording particle images at two, or more, distinct times. Our *PIV* instrumentation, Fig. 11, consists of *Nd:YAG Dual Cavity pulsed laser - Quantel Evergreen PIV 145*, which emits laser pulses with 145 mJ maximum energy and operates at 15 Hz repetition rate. A charge-coupled-device (*CCD*) camera have 2048×2048 pixels resolution and 14 frames/s frame rate. *Nikkon* lens of 50 mm focal length and an $M52$ bandpass filter are also available. The flow seeder includes a sub-micron droplet generator with inlet filter and a pressure regulator, with 4 nozzle heads, 7.10^{10} particle/s generation rate. *DaVis 8* software package is the software employed for image acquisition and data post-processing.

As stated in the paragraph above, a hot-wire anemometry system, *HWA*, employes the convective heat transfer between the fluid and the probe to provide the flow characteristics. An electric current crosses the probe/filament,

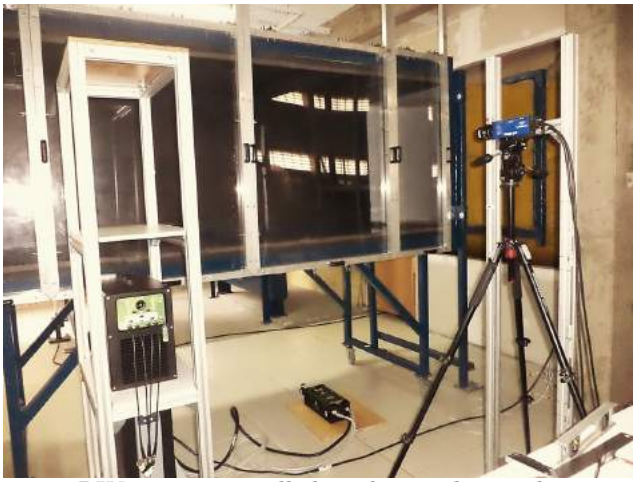

Figure 11: *PIV* system installed in the wind-tunnel test-section.

which is exposed to a cross flow, and the flow speed is evaluated through the heat transfer between the probe and the flow. The digital data acquisition system comprehends a low-pass filter for high-frequency components removal (electrical noise) and a signal conditioning unit, which aims to provide the signal obtained within the range required by the analog to digital signal converter. Our *HWA* system are under development. It comprises a series of *DISA HWA* circuits, a data acquisition systems (the same *National Instruments* employed for the aeroacoustic experiments), a probe micro-manipulator/welder, Fig. 12(a), to perform the anemometer wire repairs, and a traverse gear, Fig. 12(b), to allow the movement of the probe over the longitudinal, transverse and vertical coordinates in the test-section.

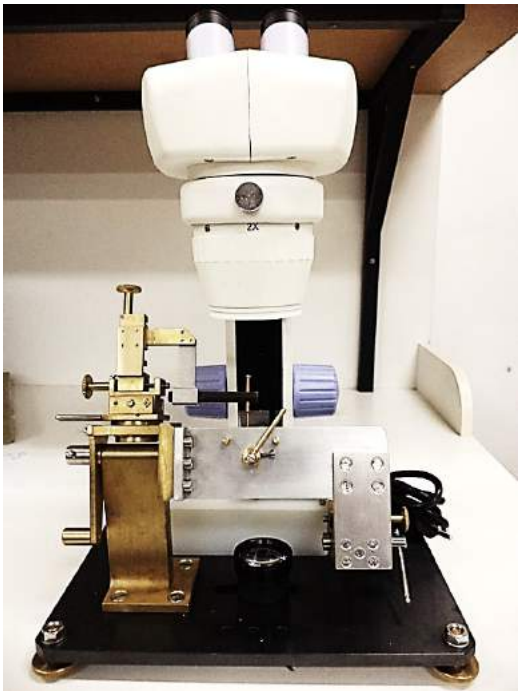

(a) Probe micro-manipulator

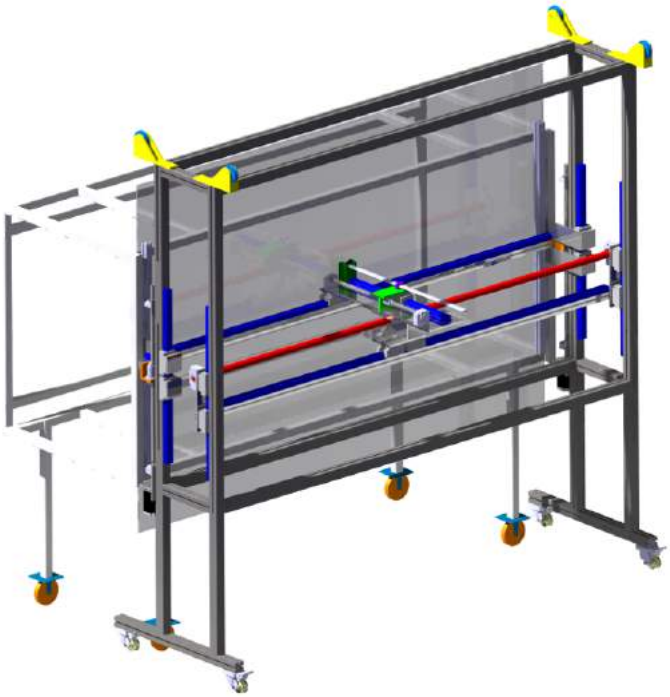

(b) Traverse gear

Figure 12: *HWA* system.

4. FINAL REMARKS

The design of a low-speed wind-tunnel has been presented in this paper. The facility accomplishes a series of features and devices to enable a low-turbulence and uniform flow, such as a special contraction shape and a long settling chamber containing screens and honeycomb devices. A low background acoustic noise was also achieved,

as the turning vanes are filled with acoustic insulation, the corners show an internal foam covering and the fan was specially designed for low noise emission levels. Such features make this facility the unique in Brazil, well suited for both aerodynamic and aeroacoustic experiments. Problems that require a low-turbulence flow, such as boundary-layer stability and transition studies, are other topics passive to be studied in this installation.

The following studies in this facility will include the test-section flow quality characterization. The microphones phased array, in combination with beamforming technique, will be employed to assess the wind-tunnel acoustic background noise, and hot-wire anemometry will determine the wind-tunnel turbulence intensity. *PIV* measurements will be made to map the flow uniformity over the test-section.

Acknowledgments

J.C.S.R. received support from from National Council for Scientific and Technological Development (CNPq/Brazil), grant #140211/2014-4. F.R.A. received funding from Coordination for the Improvement of Higher Education Personnel (CAPES/Brazil), grant #DS00011/07-0. M.A.F.M. received support from CNPq/Brazil, grant #304243/2013-2. The project financial support was provided by FINEP/Brazil, grant #01.09.0334.04.

5. REFERENCES

Amaral, F.R., Himeno, F.H.T., Pagani, Jr, C.d.C., Souza and de Medeiros, M.A.F., 2017. "Noise from the slat of an md30p30n three-element airfoil at extreme angles of attack". *submitted to AIAA Journal*.

Amaral, F.R., Pagani, Jr, C.C., Himeno, F.H.T., Souza, D.S., Alvarez, D.R. and de Medeiros, M.A.F., 2016. "Métodos de correlação cruzada em experimento e simulações do ruído acústico do eslate". In M.T. de Mendonca and A.C. Avelar, eds., *Turbulência*, Associação Brasileira de Engenharia e Ciências Mecânicas, chapter 1.

Amaral, F.R., Souza, D.S., Pagani, Jr, C.d.C. and de Medeiros, M.A.F., 2015. "Experimental study of the effect of a small 2d excrescence placed on the slat cove surface of an airfoil on its acoustic noise". In *21st AIAA/CEAS Aeroacoustics Conference*. American Institute of Aeronautics and Astronautics, AIAA Aviation. doi: doi:10.2514/6.2015-3138. URL `http://dx.doi.org/10.2514/6.2015-3138`.

Amaral, F.R., Souza, D.S., Pagani Jr., C.d.C., SerranoRico, J.C., Blanco, M. and Medeiros, M.A.F., 2014. "Estudo experimental do efeito aeroacústico de uma excrescência bidimensional na cova do eslate". In *ABCM - Anais da IX Escola de Primavera de Transição e Turbulência*. Associação Brasileira de Engenharia e Ciências Mecânicas. URL `http://abcm.org.br/app/webroot/anais/eptt/2014/eptt_anais_modificado.pdf`.

Barlow, J., Rae, W. and Pope, A., 1999. "Low-speed wind tunnel testing". *Jhon Wiley & Sons, Canada*.

Bell, J.H. and Mehta, R.D., 1988. "Contraction design for small low-speed wind tunnels". Technical Report CR-177488, NASA.

Bradshaw, P. and Pankhurst, R., 1964. "The design of low-speed wind tunnels". *Progress in Aerospace Sciences*, Vol. 5, pp. 1–69. ISSN 0376-0421.

Cattafesta, L., Bahr, C. and Mathew, J., 2010. "Fundamentals of wind tunnel design". *Encyclopedia of Aerospace Engineering*. ISSN 0470686650.

Chong, T., Joseph, P. and Davies, P., 2009. "Design and performance of an open jet wind tunnel for aero-acoustic measurement". *Applied acoustics*, Vol. 70, No. 4, pp. 605–614.

Devenport, W.J., Grissom, D.L., Nathan Alexander, W., Smith, B.S. and Glegg, S.A., 2011. "Measurements of roughness noise". *Journal of Sound and Vibration*, Vol. 330, No. 17, pp. 4250–4273. ISSN 0022-460X.

Eckert, W.T., Mort, K.W. and Jope, J., 1976. "Aerodynamic design guidelines and computer program for estimation of subsonic wind tunnel performance". Technical Report TN D-8243, NASA.

Fukano, T., Kodama, Y. and Senoo, Y., 1977. "Noise generated by low pressure axial flow fans, i: Modeling of the turbulent noise". *Journal of Sound and Vibration*, Vol. 50, No. 1, pp. 63–74.

Groth, J. and Johansson, A.V., 1988. "Turbulence reduction by screens". *Journal of Fluid Mechanics*, Vol. 197, pp. 139–155.

Hunt, L.E., Downs, R., Kuester, M. and White, E., 2010. "Flow quality measurements in the klebanoff-saric wind tunnel". *AIAA Pap. No*, Vol. 4538.

Lindgren, B., 2002. *Flow facility design and experimental studies of wall-bounded turbulent shear-flows*. Thesis, KTH.

Mathew, J., Bahr, C., Sheplak, M., Carroll, B. and Cattafesta, L.N., 2005. "Characterization of an anechoic wind tunnel facility". In *ASME 2005 International Mechanical Engineering Congress and Exposition*. American Society of Mechanical Engineers, pp. 281–285.

Mehta, R.D. and Bradshaw, P., 1979. "Desing rules for small low-speed wind tunnels". *Aeronautical Journal*, Vol. 83, No. 827, pp. 443–449. ISSN 0001-9240.

Mehta, R., 1977. "The aerodynamic design of blower tunnels with wide-angle diffusers". *Progress in Aerospace Sciences*, Vol. 18, pp. 59–120. ISSN 0376-0421.

Morel, T., 1975. "Comprehensive design of axisymmetric wind tunnel contractions". *Journal of Fluids Engineering*, Vol. 97, No. 2, pp. 225–233.

Oerlemans, S., Broersma, L. and Sijtsma, P., 2007. "Quantification of airframe noise using microphone arrays in open and closed wind tunnels". *International Journal of Aeroacoustics*, Vol. 6, No. 4, pp. 309–333. ISSN 1475-472X.

Pagani, Jr, C.d.C., 2014. *Mapeamento de Fontes Aeroacústicas de um Eslate em Túnel de Vento de Seção Fechada Utilizando Beamforming com Deconvolução DAMAS*. Thesis, Escola de Engenharia de São Carlos, Universidade de São Paulo. URL `http://www.teses.usp.br/teses/disponiveis/18/18148/tde-06122014-232641/`.

Pagani, Jr, C.d.C., Souza, D.S. and de Medeiros, M.A.F., 2016. "Slat noise: Aeroacoustic beamforming in closed-section wind tunnel with numerical comparison". *AIAA Journal*, Vol. 54, No. 7, pp. 2100–2115. ISSN 0001-1452. doi: 10.2514/1.J054042. URL `http://dx.doi.org/10.2514/1.J054042`.

Pagani, Jr, C.d.C., Souza, D.S. and de Medeiros, M.A.F., 2017. "Experimental investigation on the effect of slat geometrical configurations on aerodynamic noise". *Journal of Sound and Vibration*, Vol. 394, pp. 256–279. doi: http://dx.doi.org/10.1016/j.jsv.2017.01.013. URL `http://www.sciencedirect.com/science/article/pii/S0022460X17300111`.

Remillieux, M.C., Crede, E.D., Camargo, H.E., Burdisso, R.A., Devenport, W.J., Rasnick, M., Van Seeters, P. and Chou, A., 2008. "Calibration and demonstration of the new virginia tech anechoic wind tunnel". *AIAA*, Vol. 2911, p. 2008.

Scheiman, J. and Brooks, J., 1981. "Comparison of experimental and theoretical turbulence reduction from screens, honeycomb, and honeycomb-screen combinations". *Journal of Aircraft*, Vol. 18, No. 8, pp. 638–643.

Shin, H.C., Graham, W., Sijtsma, P., Andreou, C. and Faszer, A.C., 2007. "Implementation of a phased microphone array in a closed-section wind tunnel". *AIAA journal*, Vol. 45, No. 12, pp. 2897–2909. ISSN 0001-1452.

Tyler, J.M. and Sofrin, T.G., 1962. "Axial flow compressor noise studies". Report, SAE Technical Paper.

Watmuff, J., 1986. "Wind tunnel contraction design". In *Proceedings of 9th Australian Fluid Mechanics Conference*. pp. 82–89.

Whitehead, L.G., Wu, L.Y. and Waters, M.H.L., 1951. "Contracting ducts of finite length". *Aeronautical Quarterly*, Vol. 2, No. 4, pp. 254–271. ISSN 0001-9259. URL `<GotoISI>://WOS:A1951YA74600002`.

6. RESPONSIBILITY NOTICE

The authors are the only responsible for the printed material included in this paper.